Int J Earth Sci (Geol Rundsch) (2008) 97:1181–1200
DOI 10.1007/s00531-007-0222-y

ORIGINAL PAPER

Petrochemistry of the south Marmara granitoids, northwest Anatolia, Turkey

Zekiye Karacık · Yücel Yılmaz · Julian A. Pearce · Ö. Işık. Ece

Received: 12 May 2006 / Accepted: 19 June 2007 / Published online: 26 July 2007

Abstract Post-collision magmatic rocks are common in the southern portion of the Marmara region (Kapıdağ, Karabiga, Gönen, Yenice, Çan areas) and also on the small islands (Marmara, Avşa, Paşalimanı) in the Sea of Marmara. They are represented mainly by granitic plutons, stocks and sills within Triassic basement rocks. The granitoids have ages between Late Cretaceous and Miocene, but mainly belong to two groups: Eocene in the north and Miocene in the south. The Miocene granitoids have associated volcanic rocks; the Eocene granitoids do not display such associations. They are both granodioritic and granitic in composition, and are metaluminous, calc-alkaline, medium to high-K rocks. Their trace elements patterns are similar to both volcanic-arc and calc-alkaline post-collision intrusions, and the granitoids plot into the volcanic arc granite (VAG) and collision related granite areas (COLG) of discrimination diagrams. The have high $^{87}Sr/^{86}Sr$ (0.704–0.707) and low $^{143}Nd/^{144}Nd$ (0.5124–0.5128). During their evolution, the magma was affected by crustal assimilation and fractional crystallization (AFC). Nd and Sr isotopic compositions support an origin of derivation by combined continental crustal AFC from a basaltic parent magma. A slab breakoff model is consistent with the evolution of South Marmara Sea granitoids.

Z. Karacık (✉) · Ö.Işık.Ece
Faculty of Mines, Department of Geology,
Istanbul Technical University, Istanbul, Turkey
e-mail: zkaracik@itu.edu.tr

Y. Yılmaz
Kadir Has University, Istanbul, Turkey

J. A. Pearce
Department of Earth, Ocean and Planetary Science,
Cardiff University, Cardiff, UK

Keywords South Marmara region · Granitoids · Geochemistry · Assimilation fractional crystallization (AFC) · Slab breakoff

Introduction

The south Marmara region has a complex geology with a wide variety of metamorphic, magmatic and sedimentary rocks; their ages vary from Paleozoic to Paleogene. The general geological features of the region have been studied by several workers (i.e., Bingöl 1976; Şengör and Yılmaz 1981; Bingöl et al. 1982; Yılmaz 1990; Harris et al. 1994; Okay et al. 1996). However, only a few of these deal with some minor features of the Kapıdağ and Karabiga granitoids (Aksoy, 1995; Köprübaşı and Aldanmaz 2004).

The geology of the south Marmara region is critical to assessing the magmatic history of Western Anatolia. The objective of the present study is centered on the field aspects, petrography, geochemistry, time and space relationships, and petrogenesis of the South Marmara granitoids. We present new major and ICP-MS trace element data, together with Sr and Nd isotopic ratios and K/Ar ages for a representative suite of granitoids.

Regional geology

The northwestern part of the Turkey is delimited by the Intra-Pontide suture in the north and İzmir-Ankara suture in the south (Fig. 1). This paleotectonic unit, known as the Sakarya continent, is located in the southern part of the Marmara Sea (Şengör and Yılmaz 1981; Yılmaz 1990). Three main rock groups may be distinguished in the Sakarya continent: (1) Paleozoic–Mesozoic metamorphic basement

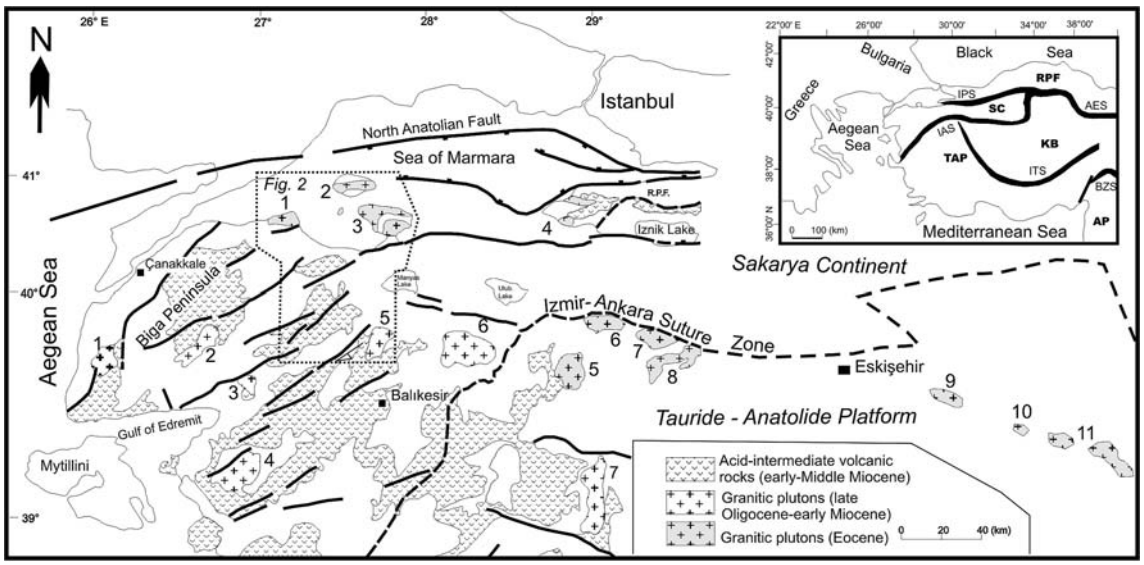

Fig. 1 The distribution of volcanic rocks and granitic plutons of northwestern Anatolia (Modified after Genç 1998; Delaloye and Bingöl 2000). Eocene plutons: *1* Karabiga pluton, *2* Marmara sill, *3* Kapıdağ pluton, *4* Fıstıklı pluton, *5* Orhaneli pluton, *6* Topuk pluton, *7* Tepeldağ pluton, *8* Göynükbelen pluton, *9* Sarıkavak pluton, *10* Kaymaz pluton, *11* Sivrihisar pluton. Miocene plutons: *1* Kestanbol, *2* Evciler, *3* Eybek, *4* Kozak, *5* Ilıca, *6* Çataldağ, *7* Eğrigöz plutons. *Inset* displays major tectonic entities and suture zones of Turkey. Abbreviations are: *IPS* Intra Pontides Suture, *AES* Ankara-Erzincan Suture, *IAS* İzmir-Ankara Suture, *ITS* Inner Tauride Suture, *BSZ* Bitlis-Zagros Suture, *RPF* Rhodope-Pontide Fragment, *SC* Sakarya continent, *TAP* Tauride-Anatolide Platform, *KB* Kırşehir Block, *AP* Arabian Platform

rocks; (2) a Cretaceous–Miocene magmatic province; and (3) Neogene sedimentary rocks (Figs. 1, 2). The metamorphic basement rocks are commonly known as the 'Karakaya Complex' (Bingöl 1976), which comprises various types of volcano-sedimentary units and tectonic blocks that have undergone low-grade and high-pressure regional metamorphism during the latest Triassic (Bingöl 1976; Yılmaz et al. 1995; Genç and Yılmaz 1997; Okay et al. 1990).

Widespread magmatic activity took place in northwestern Turkey during and following north-dipping subduction within the Neo-Tethys Ocean beneath the Sakarya continent (Şengör and Yılmaz 1981). The products of subduction-related magmatic activities are of late Cretaceous age and produced intermediate to basic volcanic rocks, intercalated with marine sediments. Subduction was followed by collision between the Sakarya continent and the Anatolide–Tauride platform to the south during the latest Cretaceous (Şengör and Yılmaz 1981; Yılmaz et al 1995). Collision-related convergence and consequent uplift continued from Paleocene to Early Miocene (Harris et al. 1994; Yılmaz et al. 1995; Okay et al. 2001). Latest Early Eocene is given as the time of onset of post-collisional extension (Yılmaz et al. 1995; Genç and Yılmaz 1997). This led to a new phase of volcanism marked by intermediate to felsic volcanism and emplacement of Eocene granites into shallow crustal levels in the eastern part of the region. To the west, volcanic rocks are absent, possibly because of deeper erosion, which affected the entire region down to the metamorphic basement during the late Eocene Oligocene period. The post-collisional granitoids intruding the basement rocks of the Sakarya continent are the Kestanbol, Evciler, Eybek, Kozak, Ilıca, Çataldağ plutons (Fig. 1) (Bingöl et al. 1982; Altunkaynak and Yılmaz 1998; Genç 1998; Karacık and Yılmaz 1998; Delaloye and Bingöl 2000; Yılmaz et al. 2001).

South Marmara granitoids (SMG)

Magmatic rocks, comprising granitic to granodioritic plutons and stocks, form a magmatic belt trending in an E–W direction. These plutons may be grouped as the South Marmara Granitoids (SMG). They may also be subdivided into as older (mainly Eocene) and younger (mainly Miocene) granitic bodies (Fig. 2). These two groups are aligned along two sub-parallel belts (Fig. 2), Eocene granites in the north and Miocene granites in the south. The Eocene granitoids comprise the Kapıdağ and Karabiga plutons, the Şevketiye stock and the Marmara sill. The Miocene granitoids are the Ilıca pluton, the Sarıoluk, Yenice and Kızıldam stocks. The latter are closely associated with intermediate to felsic volcanic rocks.

Published K/Ar radiometric age determinations for the South Marmara granitoids from the Miocene belt are listed in Table 1. In this study, 25 additional intrusive, and 6 additional extrusive, rocks were dated by the K–Ar method

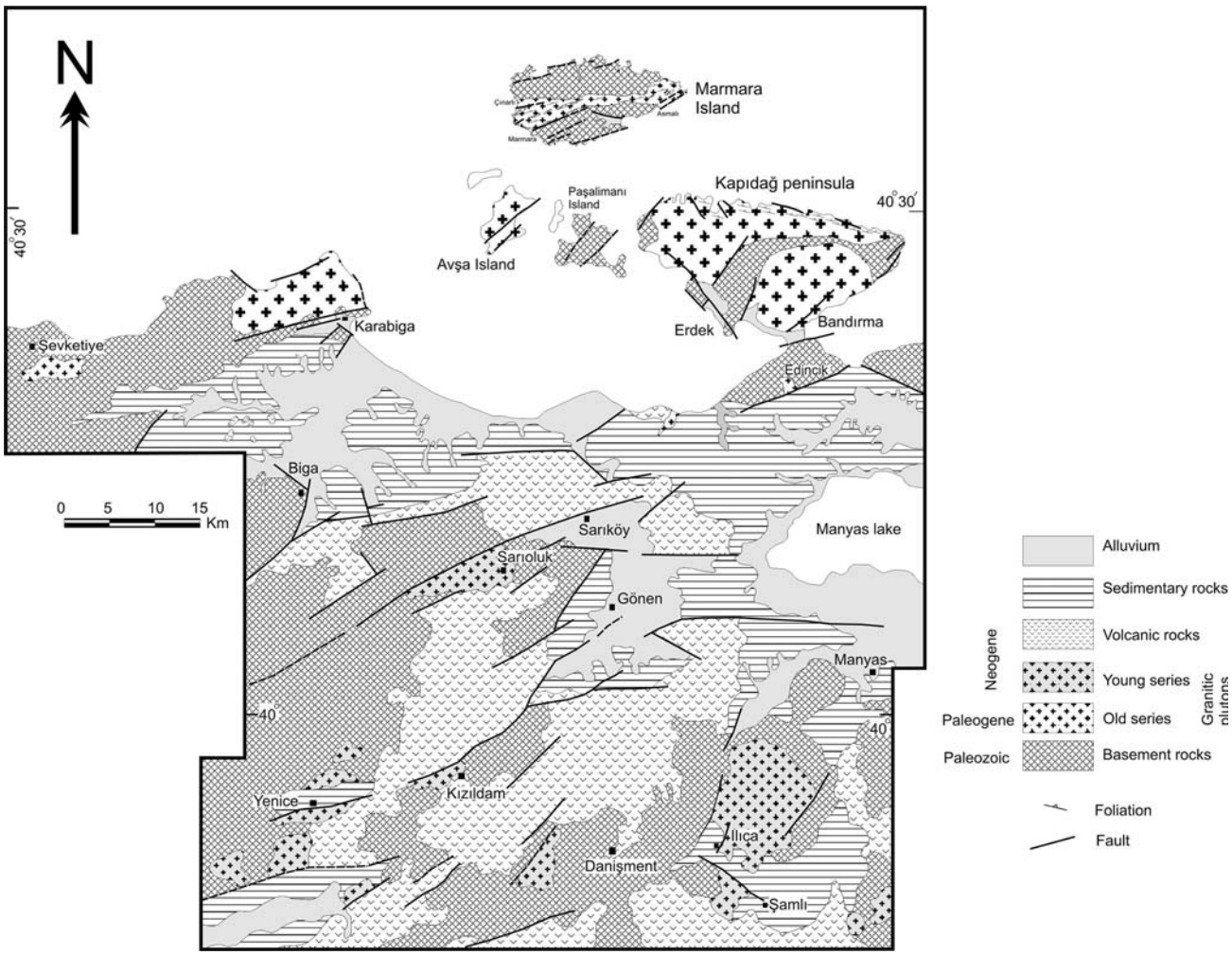

Fig. 2 Simplified geological map of the south Marmara region

Table 1 Previous geochronological data from the south Marmara granitoids

Name of intrusion	Method (K–Ar)	Age (Ma)	Authors
Kapıdağ pluton (North)	Biotite	39.9±0.8	Delaloye and Bingöl (2000)
	Hornblende	42.2±1.0	
	Biotite	38.3±0.8	
Kapıdağ pluton (South)	Biotite	38.2±0.8	Delaloye and Bingöl (2000)
	Biotite	36.1±0.8	
Karabiga	Biotite	45.3±0.9	Delaloye and Bingöl (2000)
Şevketiye	Muscovite	71.9±1.8	Delaloye and Bingöl (2000)
Ilıca-Şamlı	Orthoclase	23.1±1.2	Bingöl et al. (1982)
	Hornblende	20.3±1.1	Bingöl et al. (1982)
	Biotite	23.5±1.5	Ataman (1974)

on whole rocks and on some hornblende and biotite separates. The results are listed in Table 2. The ages of the young granitoids vary between 18.4±1.1 and 23.9±0.6 Ma. The ages of the lavas varies between 18.4±0.7 and 27.3±0.8 Ma.

The Older granitic bodies (OGB)

Among this group, the Kapıdağ granite is the largest pluton, exposed on the Kapıdağ Peninsula and Avşa Island (Fig. 2). There are also several small intrusive bodies along the coast of Marmara Sea. The Kapıdağ pluton intruded the Karakaya complex and generated a contact metamorphic aureole. The pluton comprises three different rock groups: the main body, the aplogranite rim and the locally observed foliated granite.

The main body of the pluton comprises granite and granodiorite which are light gray and massive rocks in the

Table 2 K/Ar ages for representative intrusions and lavas from the south Marmara region

Sample numbers	Location	Rock composition	Method	%K	$\%^{40}Ar_{air}$	Age Ma
ZK88	Avşa island	Granite	Biotite	7.30	5.1	40.9±1.1
ZK52	Sarıoluk	Granite	Hornblende	0.43	71.4	22.6±0.8
ZK84	Buğdaylı/Gönen	Dacite	Biotite	7.59	31.5	21.0±0.6
ZK37	Işıklı/Biga	Rhyolite	Whole rock	3.36	56.7	27.3±0.8
IE1	Yeniköy	Granite	Whole rock	2.83	31	20.1±1.0
IE2A	Davutlar	Granite	Biotite	7.00	74	21.6±0.6
IE2B	Davutlar	Granite	Whole rock	2.43	28	19.1±1.1
IE2C	Davutlar	Granite	Whole rock	2.43	27	18.4±1.1
IE3	Ilıca (South)	Dyke	Whole rock	2.62	25	19.7±1.1
IE4A	Ilıca (East)	Granite	Biotite	7.01	84	21.7±0.5
IE4B	Ilıca (East)	Granite	Whole rock	2.47	11	18.9±1.8
IE4C	Ilıca (East)	Granite	Whole rock	1.49	14	18.4±2.2
IE5A	Ilıca (West)	Granite	Biotite	7.05	91	22.8±0.5
IE5B	Ilıca (West)	Granite	Whole rock	2.44	23	19.5±1.2
IE6A	Kızıldam	Andesite	Whole rock	2.95	51	18.4±0.7
IE6B	Kızıldam	Granite	Biotite	5.41	77	23.9±0.6
IE6C	Kızıldam	Granite	Whole rock	3.25	46	20.7±0.8
IE7A	Kızıldam	Granite	Biotite	6.47	69	23.2±0.8
IE7B	Kızıldam	Granite	Whole rock	3.15	48	22.3±0.8
IE7C	Kızıldam	Granite	Whole rock	3.15	50	21.2±0.8
IE9A	Kızıldam	Granite	Biotite	6.55	86	23.4±0.6
IE9B	Kızıldam	Granite	Biotite	5.99	79	23.5±0.7
IE9C	Kızıldam	Granite	Whole rock	2.63	25	21.2±1.0
IE10A	Yenice (North)	Granite	Biotite	6.97	88	21.4±0.6
IE10B	Yenice (North)	Granite	Whole rock	3.22	18	18.8±1.3
IE10C	Yenice (North)	Granite	Whole rock	2.05	33	21.9±1.1
IE10D	Yenice (North)	Granite	Whole rock	3.44	20	20.2±1.2
IE13A	Danişment (East)	Granite	Biotite	7.28	67	23.2±1.1
IE13B	Danişment (East)	Granite	Whole rock	9.13	76	22.1±0.6
IET47A	Turplu	Andesite	Whole rock	2.67	31	19.1±1.0
IET47B	Turplu	Andesite	Whole rock	2.65	47	19.7±1.1

field. The granite is fine- to medium-grained with a granular texture, and includes sub-rounded, dioritic mafic microgranular enclaves as well as xenoliths derived from the Karakaya complex. The enclaves commonly vary from 5 to 30 cm in diameter but may, exceptionally, reach 2 m. They are fine-grained and have cuspate margins indicating that they have been produced by magma mingling. A 200 m-wide aplogranite marks the contact between the Kapıdağ granitoid and the basement rocks of the Karakaya formation. There are also numerous aplitic dikes in this region. The aplites are 20–40 cm thick and aligned in the NW–SE and NE–SW directions. The border zone also contains pegmatite dykes and porphyric veins which are dioritic in composition. One of the diorite veins is also exposed around the Edincik region, intruding the Karakaya complex. The foliated granite, located in the north of the main body, is approximately 300 m wide. The foliation is sub-parallel to the contact, and to the foliation of the underlying country rocks. The foliated granite passes gradually to non-foliated granite toward the interior of the granite body. Mafic microgranitoid enclaves are highly elongated in the foliated zone, with elongation decreasing toward the interior of the granite. The strong alignments of mafic enclaves combined with a parallel mineral alignment in the host probably formed during the emplacement of the Kapıdağ pluton. The increasing elongations of mafic enclaves toward the contact may then be explained by the expansion of the pluton during the late stage of the emplacement.

In the central part of Marmara Island, the magmatic rocks form a giant sill of predominantly dioritic composition. The Marmara Island Diorite Sill, (MIDS) extends for more than 25 km along strike and is less than 3.5 km in

width. It is a belt of broadly dioritic, sheet-like plutons striking the SW–NE and dipping steeply NW. The MIDS has steeply NW–N inclined foliation that runs parallel to the primary fabric of the country rocks. The harmonious contact relationships of the basement rocks with aureole fabric of the sill indicate that MIDS underwent the same deformation as the country rocks.

The NE–SW trending Karabiga pluton is located in the western part of the Kapıdağ pluton, which covers an area of 170 km^2. It is main lithology is white to pink granite which has a holocrystalline granophyric and porphyritic texture with K-feldspar megacrysts reaching 3 cm in length. The pluton is cut by porphyritic dacitic dykes up to 3 m wide. These dikes contain > 30% of alkali feldspar and quartz phenocrysts and abundant mafic micro-granular enclaves. The grain size decreases rapidly toward the contact, indicating rapid cooling. The Şevketiye stock is also granitic in composition and is highly altered.

The older granitic bodies range in composition from diorite to granite with major components of quartz and plagioclase (oligoclase-andesine). They are accompanied by minor hornblende, K-feldspar (orthoclase-perthite) and variable amounts of biotite. Epidote, chlorite, sericite and clay minerals are secondary in origin. Accessory minerals include apatite, sphene, zircon and opaque phases. The granitoids have a holocrystalline, hipidiomorphic granular and/or porphyritic texture. Typically granophyric and graphic textures of the aplogranite indicate that the magma reached shallow-levels in the crust. The foliated granite displays foliated textures which vary in intensity from weakly developed to gneissic.

There are metamorphic aureoles along the contact between the Karakaya complex and the South Marmara Granitoids, particularly around the Kapıdağ and Karabiga plutons. The common mineral paragenesis from the immediate contact zone outwards are: quartz + diopsite + epidote + plagioglase; quartz + diopsite + epidote + wollastonite; garnet + diopsite + wollastonite; and calcite + epidote + diopsite. These mineral parageneses indicate that hornblende hornfels–pyroxene hornfels metamorphic conditions were reached at the immediate contact, corresponding to a depth below 6 km.

The Younger granitic bodies (YGB)

The YGB is located in the southern part of the study area and is represented by a large pluton and a number of smaller intrusions together with accompanying volcanic rocks (Fig. 2). The small intrusions are the Sarıoluk, Yenice, Kızıldam, Danişment, and Yeniköy stocks. The Sarıoluk stock is the largest and covers an area of 30 km^2. The Yenice stock is the smallest with a diameter of 7 km^2. The Ilıca-Şamlı pluton covers approximately 200 km^2. All the intrusive rocks are granodioritic and monzonitic in composition. The pluton and stocks are cut by number of aplitic dykes. There is aplogranitic border zone around some stocks. The stocks contain several sub-rounded to sub-angular, dioritic microgranular enclaves and micro granite enclaves.

The Gönen volcanic association includes pyroclastic deposits and lava flows, the latter have andesite, dacite and latite compositions. They have plagioclase, hornblende, biotite and sanidine phenocrysts. The latites have sanidine megacrysts. The lavas have dioritic and micro-dioritic xenoliths.

The lavas alternate with flow breccias and lahars throughout the sequence. The volcanic sequence commonly begins at the base with pyroclastic rocks, which consist of fall and flow deposits. The fall deposits are white, displaying well-developed bedding. Their rock fragments are medium-to coarse-grained andesite, latite, perlite, rhyolite and ignimbrite clasts.

Geochemical characteristics

The geochemical classification diagrams in Fig. 3 easily distinguish the older and younger magmatic rocks and highlight the following geochemical features (Table 3).

- The SiO_2 contents of the OGB range from approximately 53 wt% (Marmara sill) to 85 wt% (Karabiga pluton). The stocks of YGB have >64 wt% SiO_2.
- The OGB are commonly low to medium K, whereas the YGB and volcanics plot in the high-K areas. Only the high silica granitoids of the OGB plot in the high-K field. The K_2O (0.26–5.35 wt%) contents of the SMG increase from north to south of the study area and correlate positively with the silica (Fig. 3a).
- All the samples are subalkaline in the total alkalis versus SiO_2 diagram of Cox et al. (1979) (Fig. 3b), with most of the OGB samples plotting within the diorite and granite fields (Fig. 3c). Two samples of the Kapıdağ pluton, both foliated granitoids, plot as diorites, and only one Marmara Island sill sample plots as gabbro. The YGB plots close to the boundary between the granite and granodiorite fields.
- On the A/CNK versus A/NK plot (Fig. 3c), the SMG samples are metaluminous with A/CNK < 1.1. The aluminum saturation index (ASI) increases with increasing SiO_2 from 0.81 to 1.10.

Variation diagrams, with silica as horizontal axis, for selected major and trace elements are given in Figs. 4 and 5. There is considerable overlap between the various granitoids for most major elements. Although individual, young plutonic bodies form clusters with little variation in SiO_2, the Gönen volcanics form linear trends for CaO,

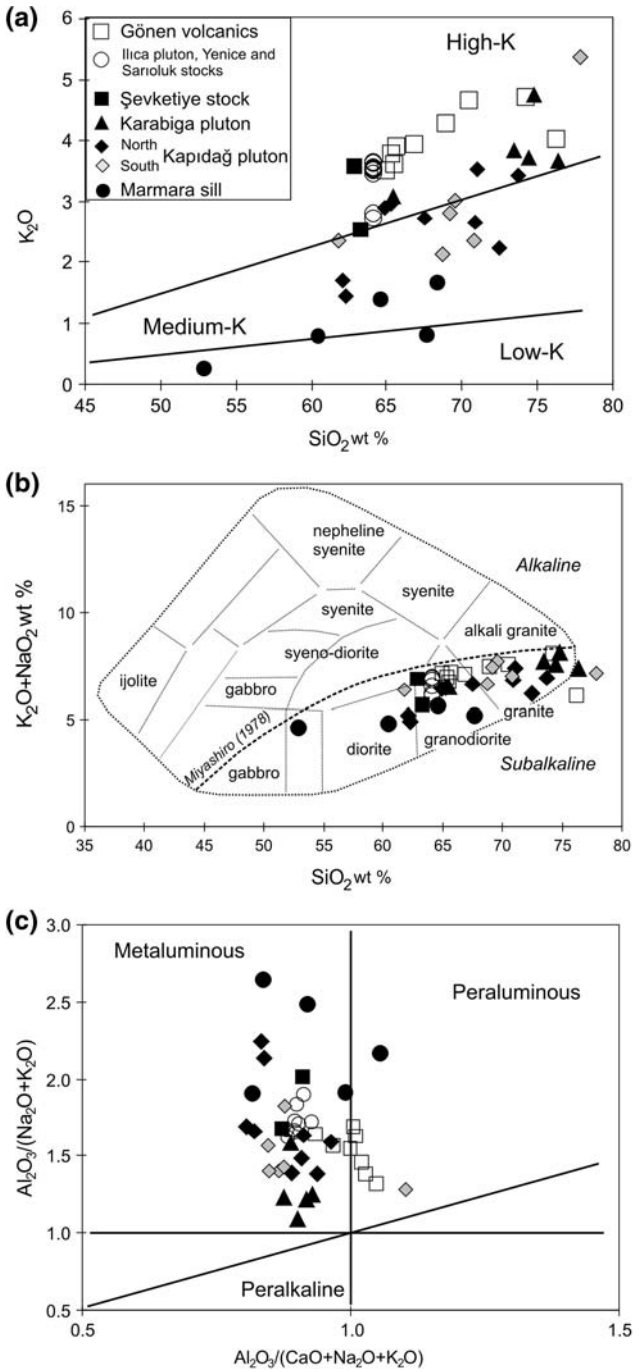

Fig. 3 **a** K_2O versus SiO_2 plot for Kapıdağ granitoids, **b** Na_2O+K_2O versus SiO_2 diagram for SMG, **c** Diagram of molar Al/Na+K versus Al/Na+K+Ca (from Maniar and Piccoli 1989) showing peraluminus character of SMG

TiO_2, total iron (as Fe_2O_3) and Al_2O_3. The South Marmara Granitoids, including both older and younger granitic bodies and volcanics, exhibit similar trends of decreasing Fe_2O_3, MgO, TiO_2, CaO and, Al_2O_3, and increasing K_2O with increasing silica. However, the CaO values of the OGB tend to be higher than the YGB at similar SiO_2. There are also different trends on SiO_2 versus Na_2O diagrams, where most of the OGB have higher Na_2O than the YGB (Table 3).

The trace element variations in Fig. 5 indicate that few elements (only Th and Rb of those shown) behave incompatibly throughout the trend from intermediate to felsic composition. For the others, the negative correlation between Y and SiO_2 for the OGB samples may be explained by fractionation of hornblende. Depletion in Sr with increasing silica for the OGB (other than the south Kapıdağ samples) may be explained by plagioclase and K-feldspar fractionation.

Older and younger plutonic bodies form distinct trends on the Th, Ba, Rb and Sr plots. Rb and Th increase markedly with increasing SiO_2 throughout the OGB, but only slightly for the YGB. The south Kapıdağ samples have higher values than the others in the Sr versus SiO_2 diagram (Fig. 5b). The Ba values of the south Kapıdağ and YGB samples are also higher than the others. Assuming that SiO_2 increases during AFC, the major and trace element variability of SMG may be explained by removal of plagioclase, and K-feldspar, together with titanite, apatite and hornblende, modified by crustal additions. The YGB and the Gönen volcanics differ from the OGB in their generally higher LIL element concentrations (K_2O, Rb, Ba and Th) and shallower AFC trends. These data thus indicate that Eocene and Miocene magmas have different histories of magmatic evolution.

Multi-element Patterns

South Marmara granitoids display somewhat similar REE patterns, with high LREE-enrichment and flat HREE (Fig. 6). Young granitoids and the Gönen volcanic rocks display greater LREE enrichment, and lower MREE and HREE contents compared with the older granitoids. The Marmara sill gives a flat pattern, and has the lowest LREE values. Most of the samples analyzed display slight Eu anomalies (northern part of the Kapıdağ and Sarıoluk) or no Eu anomalies (southern part of the Kapıdağ, Marmara and Avşa islands). In the former, the Eu anomaly is largest in the highest-silica and lowest-Sr members of the series, as found in the Karabiga pluton. This is consistent with extensive crystallization of plagioclase and alkali feldspar (Fig. 6).

Specifically, the Eu anomalies, expressed as $(Eu/Eu^*)_N$ ratios, vary between 1.1–0.9 (for the Marmara sill) and 0.4–0.9 (for the Karabiga pluton). The $(La/Yb)_N$ ratios average 12 for the Eosen granites, 6 for Marmara sill and 17 for Miocene granitoids.

The MORB-normalized trace element patterns of the SMG are shown in Fig. 7. The enrichment of the large ion lithophile elements (LILE: Sr, K, Rb, Ba, Th and U) and

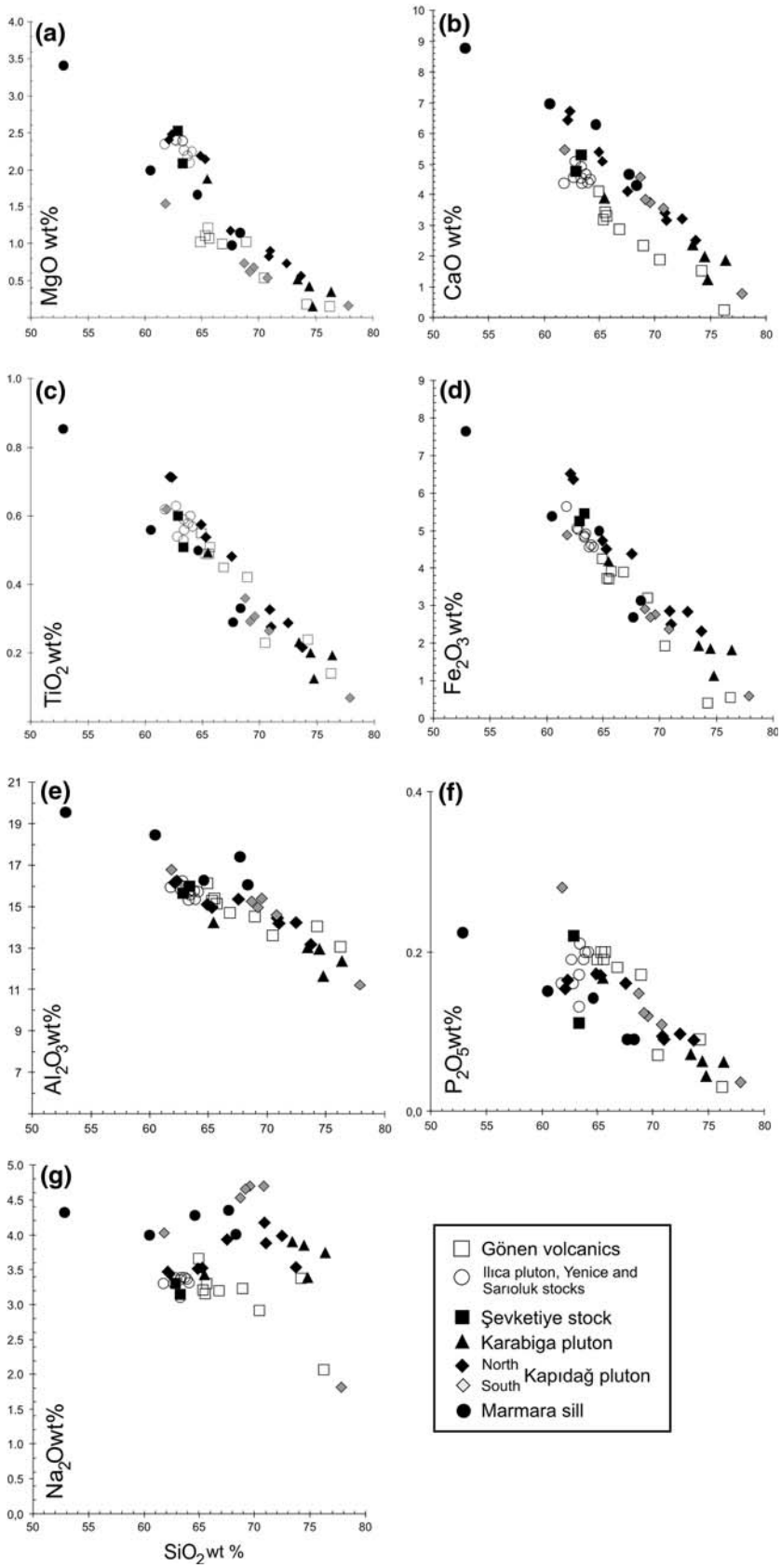

Fig. 4 Selected major element variation diagrams for the south Marmara granitoids

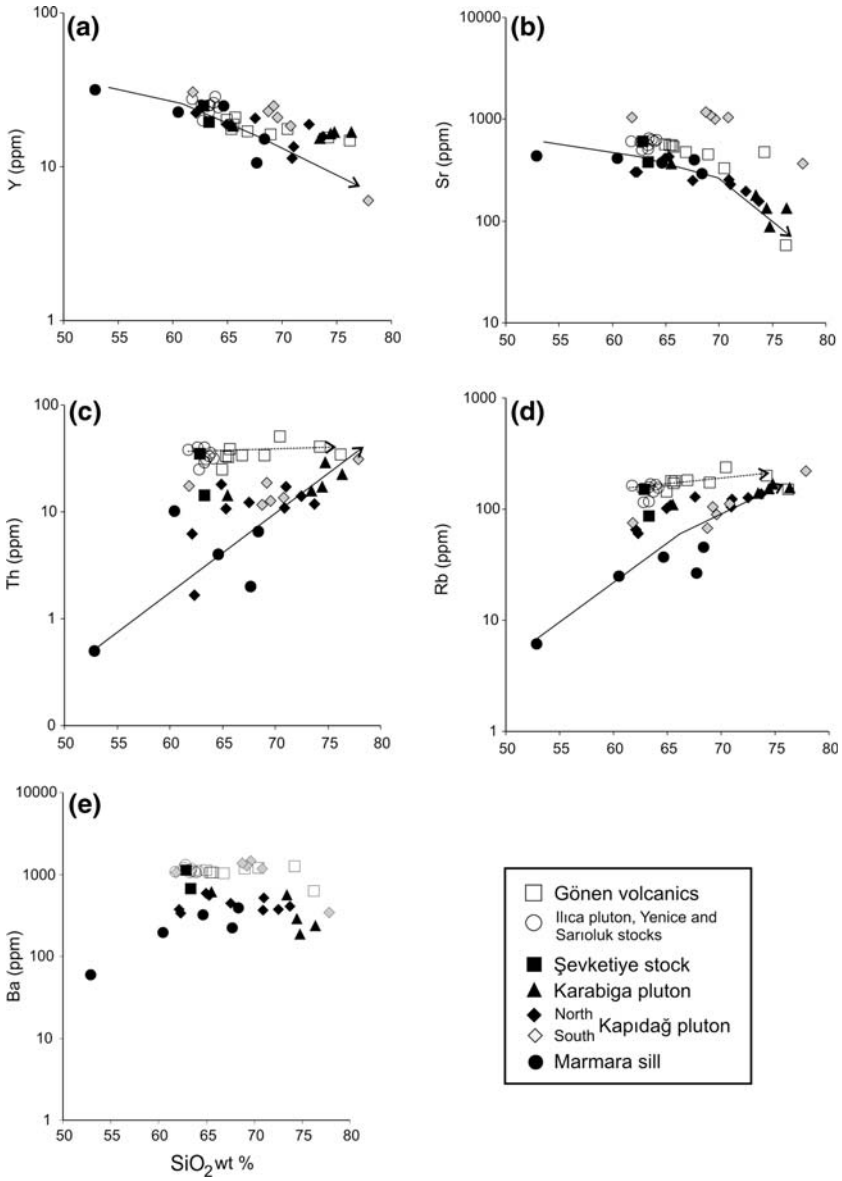

Fig. 5 Selected trace element variation diagrams for the south Marmara granitoids

depletion of high field strength elements (HFSE; Ta, Nb and Ti), and Th enrichment relative to La may attributed to a subduction-related magma pattern. However, the high La (33–56), Th (20–34), Ce (57–97), and Pb (12–19) contents of the South Marmara Granitoids, with the exception of the Marmara sill, are more characteristic of post-collisional granitoids than pure subduction-related granitoids (Harris et al. 1986; Pearce et al. 1990), whereas trace element ratios of the Marmara sill more closely resemble subduction-related magma patterns. Incorporation of continental crust may also contribute to the variability in subduction-like signatures. For example, the average Rb/Nb for the Marmara sill is about 7 which is indicative of a lesser contribution by subduction components or crustal material; the Rb/Nb averages of most other plutons have intermediate values between 9 and 10, and Karabiga Rb/Nb ratio is about 12.6, favoring incorporation of a higher crustal or subduction contribution.

The Kapıdağ granitoids can usefully be divided into high Ba–Sr granitoids and low Ba–Sr granitoids. The former are marked also by low Y (6–24 ppm), high LREEs and HREEs, low Nb and no Eu anomaly, as seen in the spider diagrams. Consequently, they have slightly high Sr/Y (34–61) and La/Yb (13–26) ratios. High Ba–Sr granitoids are known in many granitoids in Late Cretaceous and Tertiary orogenic belts worldwide (Tarney and Jones 1994).

Tectonic setting indicators

The Nb-Y and Rb-(Nb+Y) tectonic setting discrimination diagrams of Pearce et al. (1984) (Fig. 8a, b) provide a

Table 3 Whole-rock major and trace element data for the representative samples from South Marmara region

	KK82	KK80	K57	KK51	KK42	KK10	GK71	GK65	GK77	GK61	GK63
	North of Kapıdağ						South of Kapıdağ				
SiO_2	62.32	62.10	67.55	70.89	72.48	73.71	77.86	69.59	69.20	68.73	70.81
TiO_2	0.71	0.71	0.48	0.33	0.29	0.22	0.07	0.31	0.29	0.36	0.27
Al_2O_3	16.23	16.16	15.38	14.47	14.24	13.19	11.21	15.41	14.97	15.25	14.62
Fe_2O_3	6.37	6.52	4.38	2.86	2.83	2.31	0.60	2.77	2.69	2.91	2.38
MgO	2.48	2.41	1.17	0.83	0.73	0.57	0.16	0.67	0.62	0.73	0.53
MnO	0.13	0.12	0.12	0.08	0.10	0.08	0.01	0.10	0.10	0.09	0.10
CaO	6.73	6.44	4.10	3.40	3.21	2.50	0.76	3.73	3.83	4.55	3.54
K_2O	1.44	1.70	2.72	2.64	2.22	3.42	5.35	3.00	2.80	2.13	2.35
Na_2O	3.44	3.48	3.93	4.17	3.98	3.54	1.81	4.70	4.65	4.53	4.69
P_2O_5	0.16	0.15	0.16	0.09	0.10	0.09	0.04	0.12	0.12	0.15	0.11
LOI	0.42	0.46	0.51	0.53	0.47	0.47	0.80	0.37	0.40	0.40	0.21
Total	100.44	100.26	100.50	100.29	100.64	100.08	98.65	100.76	99.68	99.83	99.59
Sc	14	14	6	5	5	4	4	5	5	4	4
V	136	134	26	30	27	17	7	32	33	33	25
Cr	15	16	9	18	12	14	9	10	9	11	13
Co	16	17	12	5	5	3	1	4	4	4	3
Ni	9	19	4	14	3	7	1	7	5	18	34
Cu	8	15	21	5	5	5	5	5	6	6	4
Zn	150	1247	84	50	107	36	6	109	121	71	57
Ga	32	34	38	32	33	33	31	92	86	88	78
Rb	60	65	129	104	127	136	218	90	105	68	111
Sr	301	305	251	254	195	158	369	1004	1095	1184	1046
Y	23	23	21	11	19	16	6	21	25	23	18
Zr	132	136	160	154	145	121	51	179	182	201	174
Nb	8	9	13	9	14	11	8	14	17	16	17
Cs	3	3	6	4	10	7	3	2	2	2	6
Ba	336	373	441	365	375	404	345	1458	1283	1358	1171
La	9.76	18.86	34.98	29.25	28.44	23.92	12.26	38.57	50.24	46.76	39.87
Ce	21.12	36.37	65.42	47.80	52.14	43.78	17.11	70.40	89.79	84.42	71.17
Pr	2.84	4.19	7.05	4.70	5.54	4.68	2.14	7.64	9.56	9.21	7.58
Nd	13.08	17.03	26.65	16.43	20.72	17.49	7.13	28.85	35.39	34.91	27.97
Sm	3.32	3.64	4.96	2.78	4.09	3.45	1.07	5.23	6.20	6.34	4.97
Eu	1.08	1.14	1.17	0.82	0.86	0.76	0.33	1.57	1.76	1.87	1.47
Gd	3.40	3.60	4.28	2.41	3.62	3.02	0.85	4.43	5.20	5.31	4.10
Tb	0.53	0.54	0.57	0.31	0.50	0.42	0.11	0.56	0.67	0.66	0.52
Dy	3.61	3.57	3.45	1.85	3.07	2.55	0.66	3.35	3.95	3.83	2.99
Ho	0.75	0.73	0.66	0.35	0.58	0.48	0.15	0.63	0.76	0.71	0.55
Er	2.15	2.09	1.79	0.95	1.59	1.33	0.51	1.78	2.12	1.91	1.51
Tm	0.34	0.34	0.27	0.15	0.25	0.21	0.11	0.28	0.34	0.29	0.24
Yb	2.20	2.14	1.67	0.90	1.59	1.34	0.90	1.75	2.12	1.75	1.50
Lu	0.33	0.32	0.24	0.13	0.24	0.20	0.18	0.25	0.31	0.25	0.22
Hf	0.37	0.34	0.67	0.77	1.23	0.98	1.94	0.50	0.60	0.49	0.70
Ta	0.52	0.56	0.97	0.76	1.33	1.05	0.74	0.84	1.05	1.01	0.96
Pb	17.38	65.19	24.84	22.41	29.10	34.96	19.38	37.00	42.63	30.14	38.81
Th	1.67	6.22	12.25	10.82	14.08	11.80	30.85	12.65	18.85	11.62	13.60
U	1.05	2.07	2.36	1.69	3.98	2.38	5.19	3.60	6.49	2.16	7.23

Table 3 continued

	A-K85	A-K88	A-K86	MK102	M-K97	M-13	M-12	M-93	K107	K124	K123	K132	K110	K111
	Avşaisland			Marmaraisland					Karabiga					
SiO_2	65.30	71.03	64.92	52.87	64.63	60.47	67.69	68.36	85.00	74.46	76.36	74.76	73.43	65.49
TiO_2	0.54	0.28	0.58	0.85	0.50	0.56	0.29	0.33	0.01	0.20	0.19	0.13	0.23	0.49
Al_2O_3	14.97	14.19	15.10	19.54	16.28	18.46	17.40	16.07	13.34	12.96	12.38	11.64	13.04	14.24
Fe_2O_3	4.51	2.50	4.74	7.64	5.00	5.39	2.68	3.13	1.52	1.85	1.81	1.13	1.93	4.19
MgO	2.14	0.90	2.19	3.41	1.66	2.00	0.97	1.14	0.26	0.43	0.35	0.15	0.51	1.87
MnO	0.10	0.08	0.10	0.14	0.15	0.13	0.07	0.1	0.08	0.07	0.07	0.03	0.08	0.11
CaO	5.08	3.16	5.39	8.78	6.28	6.96	4.64	4.3	0.60	1.98	1.85	1.22	2.37	3.87
K_2O	2.95	3.52	2.90	0.26	1.38	0.78	0.80	1.66	0.01	3.71	3.66	4.74	3.84	3.08
Na_2O	3.53	3.88	3.51	4.32	4.27	4.00	4.35	4.01	0.03	3.85	3.75	3.38	3.90	3.43
P_2O_5	0.17	0.09	0.17	0.22	0.14	0.15	0.09	0.09	0.06	0.06	0.06	0.04	0.07	0.17
LOI	0.64	0.41	0.62	1.49	0.58	1.00	0.90	0.70	0.29	0.27	0.25	0.25	0.48	2.82
Total	99.93	100.02	100.22	99.52	100.88	99.90	99.88	99.89	101.20	99.84	100.72	97.49	99.88	99.76
Sc	11	4	11	16	9	8	4	4	2	2	3	3	4	8
V	102	39	107	180	105	36	18	42	12	20	20	8	24	84
Cr	23	12	17	37	11	–	–	–	9	11	11	9	14	20
Co	12	5	12	19	11	12	5	6	2	2	3	2	3	10
Ni	7	13	47	39	9	3	1	2	19	4	2	3	1	12
Cu	9	7	12	26	16	11	6	25	4	5	4	7	5	17
Zn	52	132	53	66	163	47	43	48	25	69	28	293	28	63
Ga	40	38	42	20	32	20	15	15	22	25	23	20	39	42
Rb	108	122	102	6	37	25	27	46	183	153	156	168	139	110
Sr	429	229	417	434	375	417	402	292	88	134	133	88	181	364
Y	19	13	19	32	25	23	11	15	18	16	17	17	15	18
Zr	144	113	99	163	112	115	95	95	3	129	144	79	106	162
Nb	11	11	10	2	3	2	2	2	14	11	13	15	10	12
Cs	3	3	3	0	1	1	1	1	5	3	3	4	3	2
Ba	550	521	585	60	320	195	223	393	217	287	237	188	559	610
La	32.65	18.73	30.16	5.66	14.54	39.00	7.60	25.60	29.01	27.84	31.01	32.39	29.49	28.31
Ce	56.30	31.48	54.70	14.51	28.14	77.60	16.10	46.30	48.42	43.38	50.79	53.33	46.09	52.56
Pr	5.87	3.22	5.85	2.39	3.42	8.10	1.98	4.64	4.67	4.16	4.86	5.32	4.41	5.70
Nd	21.93	11.59	22.05	12.89	14.57	29.90	8.80	17.50	15.45	13.76	15.96	17.67	14.67	21.74
Sm	4.14	2.22	4.21	3.93	3.34	4.30	1.60	2.70	2.71	2.34	2.70	3.11	2.45	4.17
Eu	1.18	0.71	1.21	1.28	1.11	1.22	0.56	0.72	0.40	0.51	0.50	0.37	0.69	1.15
Gd	3.73	2.08	3.74	4.27	3.38	3.75	1.62	2.32	2.50	2.24	2.40	2.64	2.27	3.67
Tb	0.49	0.29	0.50	0.71	0.53	0.63	0.28	0.41	0.37	0.32	0.34	0.37	0.32	0.49
Dy	3.01	1.92	3.05	4.97	3.63	3.35	1.50	2.24	2.47	2.18	2.27	2.28	2.09	3.02
Ho	0.59	0.40	0.60	1.05	0.78	0.73	0.33	0.76	0.54	0.47	0.48	0.47	0.45	0.59
Er	1.66	1.21	1.69	3.03	2.30	2.30	1.05	1.49	1.72	1.50	1.53	1.47	1.37	1.65
Tm	0.26	0.21	0.27	0.49	0.39	0.34	0.17	0.25	0.32	0.27	0.28	0.27	0.25	0.27
Yb	1.70	1.44	1.70	3.10	2.59	2.44	1.30	1.60	2.27	1.92	1.98	1.98	1.69	1.71
Lu	0.26	0.23	0.26	0.46	0.41	0.35	0.21	0.25	0.38	0.32	0.33	0.33	0.27	0.26
Hf	0.86	0.83	0.81	0.52	0.50	3.35	2.80	2.70	2.09	0.96	1.13	1.54	0.97	1.50
Ta	0.81	1.23	0.76	0.08	0.22	0.10	0.10	0.20	1.61	1.08	1.35	1.80	0.88	0.88
Pb	20.84	39.11	21.54	6.68	18.61	1.30	1.20	1.90	29.28	22.39	21.05	40.19	23.25	22.09
Th	10.70	17.17	17.98	0.50	3.99	10.10	2.00	6.60	27.98	17.23	22.37	29.06	15.85	14.33
U	3.12	5.78	3.51	0.35	0.99	1.00	0.80	1.10	4.59	3.32	3.30	2.68	3.60	2.93

Table 3 continued

	S-65	S-66	SO-52	SO-54	I-4	I-5	K-6	K-7	K-8	Y-10	Y-11
	Şevketiye		Sarıoluk		Ilıca		Kızıldam			Yenice	
SiO_2	62.85	63.32	64.13	63.73	63.32	62.77	63.31	62.64	61.74	63.9	63.4
TiO_2	0.6	0.51	0.57	0.58	0.53	0.54	0.59	0.63	0.62	0.6	0.56
Al_2O_3	15.66	16	15.72	15.75	15.76	16.23	15.33	15.84	15.95	15.38	15.60
Fe_2O_3	5.26	5.47	4.58	4.58	4.87	5.04	4.83	5.07	5.64	4.63	4.92
MgO	2.53	2.09	2.25	2.19	2.39	2.4	2.4	2.41	2.35	2.1	2.27
MnO	0.1	0.18	0.09	0.08	0.1	0.09	0.09	0.09	0.11	0.09	0.08
CaO	4.75	5.3	4.48	4.65	4.92	5.09	4.53	4.56	4.37	4.38	4.36
K_2O	3.57	2.53	3.64	3.53	2.81	2.72	3.46	3.51	3.52	3.62	3.56
Na_2O	3.31	3.15	3.32	3.39	3.36	3.39	3.11	3.31	3.31	3.37	3.39
P_2O_5	0.22	0.11	0.2	0.19	0.13	0.16	0.17	0.19	0.16	0.2	0.21
LOI	0.9	1.2	0.8	1.1	1.5	1.3	1.9	1.7	1.9	1.4	1.3
Total	99.89	99.94	99.91	99.9	99.69	99.73	99.72	99.95	99.67	99.67	99.65
Sc	10	9	9	9	11	10	12	11	11	10	11
V	108	112	98	93	112	112	104	108	109	107	118
Cr	–	–	–	–	–	–	–	–	–	–	–
Co	13	12	11	11	120	33	43	32	40	47	142
Ni	<20	<20	<20	<20	4	3	6	7	7	6	7
Cu	24.2	155.6	25.7	15.0	5	14	6	16	33	6	8
Zn	41	108	37	34	34	26	18	26	37	30	27
Ga	20	18	19	19	19	18	17	18	18	18	19
Rb	150	87	155	143	117	115	158	154	163	166	169
Sr	610	383	632	632	513	506	557	602	612	604	657
Y	25	20	24	26	23	20	25	25	27	28	25
Zr	167	107	175	213	136	133	176	174	161	166	185
Nb	14	8	15	15	12	11	16	15	16	18	16
Cs	8	2	8	6	5	5	17	6	9	5	6
Ba	1118	666	1106	1095	1102	1322	1057	1191	1077	1054	1171
La	54.30	25.20	53.40	56.40	47.80	32.90	55.10	55.70	61.20	66.40	74.50
Ce	97.60	42.10	97.70	100.70	77.90	58.00	97.10	100.00	110.00	113.50	118.30
Pr	10.75	4.46	10.69	11.59	7.77	6.04	10.33	10.18	11.55	11.67	11.41
Nd	40.90	16.90	41.60	43.40	27.60	22.70	40.20	39.30	44.70	44.50	42.80
Sm	7.10	3.40	7.70	7.50	4.80	4.40	6.80	6.90	8.10	7.70	7.40
Eu	1.44	0.89	1.42	1.39	1.17	1.07	1.34	1.41	1.56	1.57	1.47
Gd	5.13	3.09	4.77	5.46	4.20	3.90	5.11	5.20	6.25	6.01	5.66
Tb	0.72	0.47	0.72	0.69	0.63	0.55	0.76	0.75	0.82	0.85	0.79
Dy	3.64	2.62	3.63	4.19	3.56	3.16	4.00	4.02	4.62	4.73	4.28
Ho	0.70	0.57	0.72	0.77	0.74	0.66	0.81	0.80	0.89	0.89	0.80
Er	2.13	1.82	2.31	2.24	2.12	2.06	2.39	2.39	2.57	2.63	2.39
Tm	0.37	0.29	0.33	0.40	0.32	0.29	0.34	0.34	0.39	0.40	0.36
Yb	2.08	2.04	2.58	2.46	2.22	2.02	2.37	2.27	2.62	2.79	2.36
Lu	0.39	0.32	0.38	0.40	0.34	0.32	0.39	0.38	0.39	0.42	0.39
Hf	4.50	3.10	4.30	5.80	4.10	4.20	5.50	5.10	4.60	5.00	5.60
Ta	1.30	0.80	1.60	1.50	1.50	1.20	1.70	1.40	1.80	1.90	1.90
Pb	27.2	50.6	25.9	17.4	14.50	4.90	16.30	21.70	30.80	7.80	9.80
Th	34.90	14.20	31.70	33.40	29.00	25.10	40.00	40.10	37.80	35.70	31.20
U	11.90	4.70	10.60	11.00	5.80	7.40	13.50	10.80	11.80	9.60	9.80

Table 3 continued

	ZK-02–05	ZK-02-09	ZK-02-12	ZK-02-16	ZK-02-17	ZK-02-23	ZK-02-37	ZK-02-70	ZK-02-81	ZK-02-84
	Gönenvolcanics									
SiO_2	66.84	65.7	65.56	70.46	65.35	74.22	76.23	61.81	64.94	68.95
TiO_2	0.45	0.51	0.49	0.23	0.49	0.24	0.14	0.62	0.55	0.42
Al_2O_3	14.72	15.13	15.4	13.62	15.3	14.05	13.07	16.79	16.14	14.52
Fe_2O_3	3.89	3.91	3.71	1.92	3.73	0.4	0.56	4.88	4.26	3.2
MgO	0.99	1.07	1.21	0.53	1.11	0.18	0.15	1.54	1.02	1.02
MnO	0.03	0.08	0.07	0.05	0.07	–	–	0.15	0.11	0.04
CaO	2.86	3.29	3.41	1.87	3.17	1.51	0.25	5.48	4.09	2.34
K_2O	3.93	3.9	3.6	4.65	3.77	4.7	4.01	2.35	3.51	4.28
Na_2O	3.2	3.31	3.16	2.92	3.21	3.38	2.06	4.03	3.66	3.23
P_2O_5	0.18	0.2	0.19	0.07	0.2	0.09	0.03	0.28	0.19	0.17
LOI	2.7	2.7	3	3.5	3.4	1	3.4	1.8	1.3	1.6
Total	99.91	99.92	99.93	99.96	99.92	99.92	99.98	99.84	99.9	99.91
Sc	6	8	7	3	7	2	2	5	8	5
V	56	70	86	25	59	13	7	71	79	51
Cr	–	–	–	–	–	–	–	–	–	–
Co	6	10	10	3	10	1	2	7	13	6
Ni	<20	20	<20	<20	<20	<20	76	<20	23	<20
Cu	14.7	15.3	9.1	2.6	11.0	2.1	0.5	3.9	13.2	6.8
Zn	42	42	44	17	33	4	4	53	47	38
Ga	17	19	19	17	19	19	14	23	19	18
Rb	183	180	170	239	179	200	150	76	144	175
Sr	477	533	561	329	552	474	58	1033	568	454
Y	17	21	19	18	18	16	15	31	20	16
Zr	171	182	178	154	173	166	97	201	181	173
Nb	17	18	17	16	17	19	23	15	15	18
Cs	8	8	7	13	7	8	9	3	6	6
Ba	1035	1060	1066	1204	1053	1253	630	1051	1121	1177
La	53.30	55.80	54.20	61.90	54.50	68.20	34.20	57.70	50.40	52.80
Ce	82.70	95.60	93.10	97.90	93.60	107.50	54.90	102.80	83.50	77.60
Pr	8.73	9.47	8.77	8.74	9.11	10.40	5.28	12.10	8.83	8.52
Nd	30.90	32.50	32.20	30.90	33.10	34.80	19.10	46.50	31.50	28.00
Sm	5.20	6.10	6.00	4.30	5.40	5.20	3.60	7.40	5.70	4.50
Eu	1.00	1.33	1.13	0.85	1.08	1.06	0.48	1.98	1.18	0.90
Gd	3.56	4.58	3.78	2.98	3.54	3.29	2.13	6.61	4.05	3.52
Tb	0.51	0.53	0.54	0.44	0.50	0.40	0.35	0.82	0.56	0.52
Dy	2.55	3.33	2.76	2.46	2.93	2.41	2.25	4.56	3.02	2.52
Ho	0.49	0.64	0.58	0.46	0.58	0.44	0.37	0.89	0.70	0.48
Er	1.36	1.87	1.56	1.47	1.49	1.32	1.17	2.73	1.87	1.38
Tm	0.25	0.29	0.29	0.25	0.22	0.23	0.24	0.44	0.32	0.24
Yb	1.66	1.87	1.76	2.08	1.95	1.47	1.66	3.15	1.89	1.42
Lu	0.27	0.34	0.26	0.32	0.28	0.27	0.25	0.44	0.29	0.25
Hf	5.00	4.30	4.30	4.60	4.50	4.40	3.20	5.20	4.60	5.30
Ta	1.60	1.70	1.40	1.40	1.40	1.60	1.90	1.00	1.30	1.70
Pb	1.9	7.1	9.7	1.9	9.7	13.4	4.3	5.7	9.1	5.7
Th	33.70	38.70	32.70	51.00	33.40	40.50	34.60	17.40	25.10	33.60
U	5.40	7.60	8.30	13.90	7.30	12.90	6.80	4.70	7.60	8.50

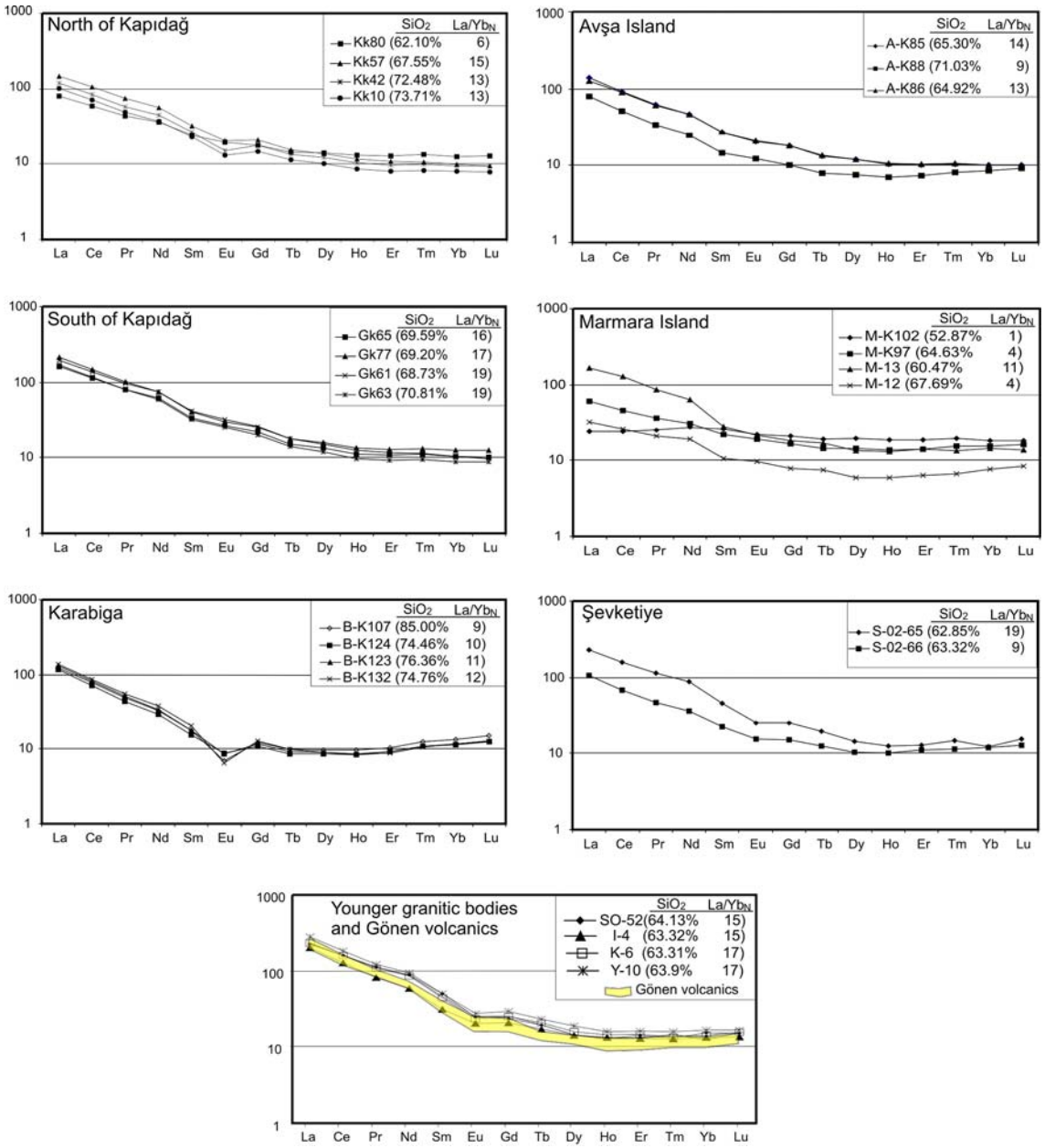

Fig. 6 Chondrite-normalized REE abundance patterns (normalizing ratios are from Sun and McDonough (1989)) for representative samples from the SMG

means to compare the SMG in a tectonic context. The SMG plot within the syn-collisional granite (syn-COLG) + volcanic arc granite (VAG) field on the Nb–Y diagram. In the Rb–(Y+Nb) diagram, the samples plot in the upper part of the VAG field; however, most also plot in the same field as post-collisional granitoids. In order to determine these two tectonic settings trace-element discrimination diagrams are further used. To distinguish VAG from post-COLG, the Rb–Hf–Ta ternary diagram may be used (Harris et al. 1986) (Fig. 9). The SMG data plot in three different fields on this diagram. Most of the Eocene granitoids plot within syn-collisional field; the Miocene granitoids plot within late- and post-collision granites. Three samples of Marmara sill plot in the volcanic arc field, with only one sample in the syn-collisional field. A few samples plot close to the boundary separating the volcanic arc field from late- and post-collision field.

Isotope geochemistry

Sr and Nd isotope ratios determined in this study are listed in Table 4, represented in Figs. 10 and 11. The $^{87}Sr/^{86}Sr$ ratios ranges from 0.704 to 0.707 and $^{143}Nd/^{144}Nd$ ratios

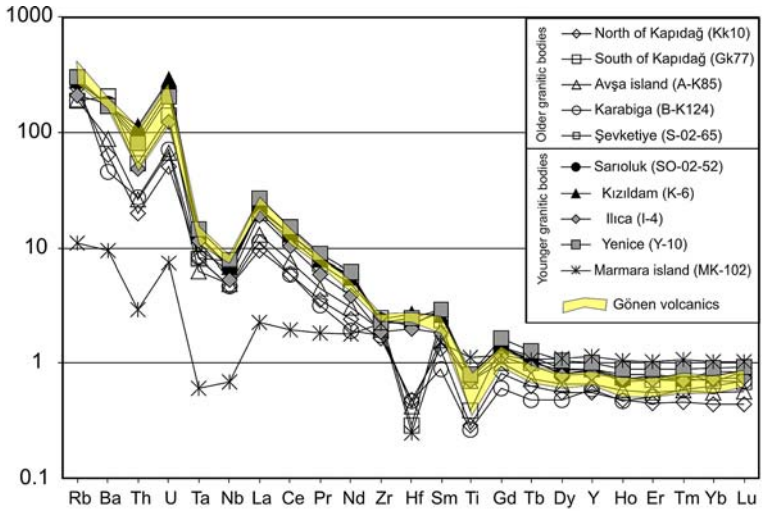

Fig. 7 N-type MORB-normalized trace element patterns in representative samples from the SMG. N-MORB values are taken from Sun and McDonough (1989), ordered by Pearce (1983)

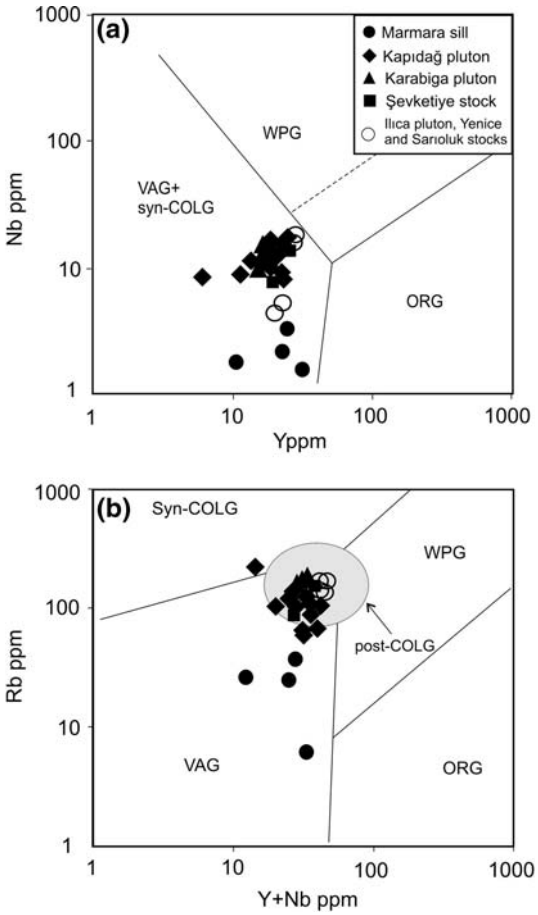

Fig. 8 **a** Nb versus Y and **b** Rb versus Y + Nb discrimination diagrams for SMG

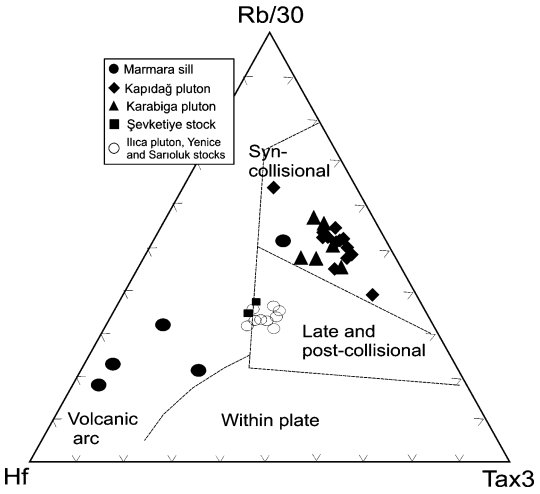

Fig. 9 Rb–Hf–Ta triangular plot for SMG (Harris et al. 1986)

range from 0.51242 to 0.5129 for the SMG. Initial ratios were calculated using ages of 40 Ma for the Kapıdağ, Karabiga plutons, and 25 Ma for the Sarıoluk granites and Gönen volcanics. The initial $^{87}Sr/^{86}Sr$ and $^{143}Nd/^{144}Nd$ ratios of the south Marmara granitoids and Gönen volcanics are plotted against SiO_2 to assess the importance of AFC and source enrichment processes. Aegean Miocene volcanic samples (Ayvacık, Bergama and Bigadiç volcanics) have also been plotted on these diagrams for the comparison purpose (Fig. 10a, b). They plot clearly above the SMG samples. Increasing $^{87}Sr/^{86}Sr_i$ and decreasing $^{143}Nd/^{144}Nd_i$ ratios with increasing SiO_2 imply an AFC process for the generation of both Old and Young series granitoids (Taylor 1980; De Paolo 1981; Thirlwall and Jones 1983; Hawkesworth 1982; Gülen 1990; Güleç 1991). The ratio of the rates of mass assimilation to mass crystallization (r) values gradually increases from Marmara samples (r = 0.1–0.2) to Aegean Miocene volcanic samples (r = 0.4–0.6) in Fig. 10a, b.

The basement below the Western Anatolia, as crop out in numerous inliers such as Kazdağ, Uludağ and Karakaya complexes are represented by high-grade metapelitic and

Table 4 Sr and Nd isotope data for the representative South Marmara granitoids and Gönen volcanics

Sample number	Location	SiO_2 (wt%)	Rb (ppm)	Sr (ppm)	$^{87}Rb/^{86}Sr$	$^{87}Sr/^{86}Sr$	$^{87}Sr/^{86}Sr(i)$	Sm (ppm)	Nd (ppm)	$^{147}Sm/^{144}Nd$	$^{143}Nd/^{144}Nd$	$^{143}Nd/^{144}Nd$ (i)	eNd(T)	eNd(0)
ZK-51	Kapıdağ	70.89	104	254	1.18454	0.70682	0.70615	2.8	16.4	0.10274	0.51258	0.51256	–0.6	–1.0
ZK-61	Kapıdağ	68.73	67.5	1184	0.16491	0.70605	0.70596	6.3	34.9	0.11028	0.51251	0.51249	–1.9	–2.3
ZK-97	Marmara	64.63	37.1	375	0.28616	0.70500	0.70481	3.3	14.6	0,13921	0.51285	0.51281	4.6	4.2
ZK-102	Marmara	52.87	6.1	434	0.04065	0.70431	0.70428	3.9	12.9	0.18515	0.51290	0.51285	5.2	5.1
ZK-110	Karabiga	73.43	139	181	2.22173	0.70700	0.70557	2.4	14.7	0.10141	0.51260	0.51257	–0.2	–0.7
ZK-52	Sarıoluk	64.13	155	631	0.71067	0.70730	0.70703	7.7	41.6	0.11239	0.51247	0.51246	–2.8	–3.1
ZK-9	Gönen	65.70	180	533	0.97702	0.70709	0.70680	6.1	32.5	0.11397	0.51250	0.51248	–2.5	–2.7
ZK-23	Gönen	74.22	200	474	1.22080	0.70784	0.70737	5.2	34.8	0.09073	0.51242	0.51240	–3.8	–4.2

metabasic metamorphic rocks (Yılmaz 1990, 1997; Genç and Yılmaz 1995; Okay and Satır 2000) but we do not have isotope values for these bodies. Therefore, we use, for the Fig. 10, the values derived from central Europe crust composition (Voshage et al. 1990). The most primitive sample (Kula basalts) is chosen as the parental magma for these rocks.

The high Sr isotope ratio of the Kapıdağ and Karabiga plutons indicates that there are two components; (1) the subduction component and (2) crustal component. Young granitoids, represented by the Sarıoluk stock and the Gönen volcanics plot in the same field as the Miocene volcanic samples.

The variations in the $^{87}Sr/^{86}Sr$ and $^{143}Nd/^{144}Nd$ ratios of the SMG are compared with Bulk Earth and the mantle array in Fig. 11. The Marmara sill samples plot closest to the mantle array which is compatible with the positive ε_{Nd} values of the rocks (Table 4); implies that magma derived from an isotopically depleted source. Low $^{87}Sr/^{86}Sr$ and high $^{143}Nd/^{144}Nd$ and low Nb, Ba and Rb content indicate a mantle source also for the Marmara sill.

The higher $^{87}Sr/^{86}Sr$ and the lower $^{143}Nd/^{144}Nd$ isotope ratios of the South Marmara Granitoids may be interpreted in terms of crust–magma interaction, as seen clearly as the samples plot along the arrow. To clarify this view, the mixing hyperbole constructed between the depleted mantle derived magma as exemplified by the Kula basalts which are known to be the most primitive basalts for the western Anatolia (TM-9-67) (Güleç 1991) and upper continental crust (Goldstein et al. 1984) are drawn using a model, developed by Langmuir et al. (1978) (Fig. 11). On the basis of these calculations the crustal component in the magma is approximately 10–15% for Marmara sill, 40% for the Kapıdağ and Karabiga granitoids and 50–60% for the Young series stocks and lavas. The ratio falls into the range given in the neighboring regions for Aegean Miocene volcanics (Aldanmaz et. al. (2000); Güleç (1991).

Discussion

Higher $^{87}Sr/^{86}Sr$ ratio indicates that younger granites have experienced greater crustal input than older granites. In the latter, the crustal components may be estimated to be about 50% p.c. (Fig. 11). When all the isotope data are collectively evaluated it may be concluded that the crustal contribution is greater in the Miocene than in the Eocene. The older granites have lower Sr and higher Nd isotope ratios but the Marmara sill has significantly lower Sr isotope ratios than the others, which indicates that they may have been derived from a depleted mantle source. A narrow and similar range of Nd–Sr isotope compositions of both the young series stocks and Gönen volcanics is consistent with

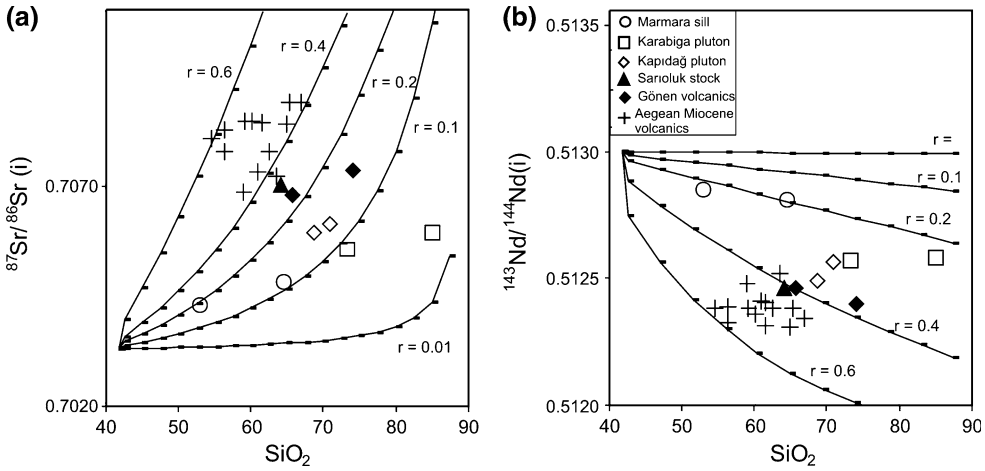

Fig. 10 **a** $^{87}Sr/^{86}Sr$ (i) versus SiO_2, **b** $^{143}Nd/^{144}Nd$ (i) versus SiO_2 diagrams for SMG. The *r* values denote the ratio of the rates of mass assimilation to mass crystallization

a comagmatic origin for the different magma batches, which show significant assimilation of crustal materials during magma ascent and intrusion at upper crustal levels. The correlations between isotope ratios and silica are clearly compatible with an AFC model. Crustal contributions are 10–20% for the Marmara sill, which are the most primitive magmas in the region, increasing towards the south. The crustal contribution averages ~40% for the Kapıdağ and Karabiga plutons and 50–60% for young stocks and Gönen volcanic rocks.

The obvious explanation for increased crustal input in the Miocene compared to the Eocene is an increase in crustal thickening and in the crustal geotherm. Geological evidence for the increase in crustal thicknesses from late Eocene to Early Miocene is discussed extensively for Western Anatolia by Şengör et al. (1984) and Yılmaz (1989). The data for these may be summarized as follows; a gradual transition from marine deposits to continental deposits is evident from Eocene to Oligocene–Early Miocene in northwestern Anatolia and Thrace. No marine deposits were formed during the Oligocene period in the northwestern Anatolia. The late Eocene–Oligocene and Early Miocene volcanoclastic succession were also formed under subaerial conditions. The region experienced an intense phase of subaerial erosion during the late Eocene–Oligocene period (Şaroğlu et al. 1992; Emre et al. 1997; Yılmaz et al. 2000). The transition of the marine sediments to the continental deposits is associated with the N–S trust tectonic and the consequent crustal thickening.

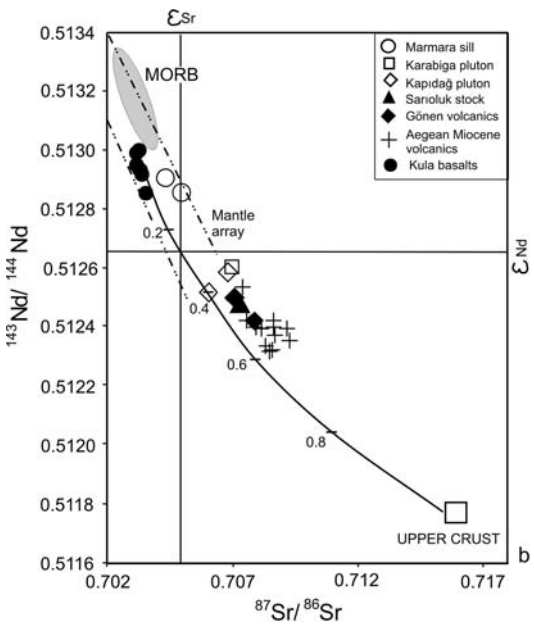

Fig. 11 $^{87}Sr/^{86}Sr$ with $^{143}Nd/^{144}Nd$ in the magmatic rocks of south Marmara region. The *numbers* on the hyperbole represents ratios of the crustal materials in the magma. Aegean Miocene volcanics are taken from Aldanmaz et al. (2000) and Güleç (1991)

The evolutions of felsic magmatism in some continental margins have been explained by the combined effects of fractional crystallization from mantle derived basalt by crustal assimilation, magma replenishment, and mixing. Base-level mixing of subcrustal and deep crustal magmas in zones of melting, assimilation, storage, and homogenization (MASH) at the mantle–crust transition is also widely occurred (Hildreth and Moorbath 1988; Grove et al. 1997). These models generally require a substantial crustal component, estimated at ~50% of crustal and mantle components for the huge Sierra Nevada and Peninsular Ranges calc-alkaline batholiths of California (De Paolo 1981); likewise Grove et al. (1997) estimated 55–60% or more for rhyolites at Medicine Lake, California. The crustal contribution obtained here, of nearly 50% for the South Marmara Granitoids, is as similar as active continental margins.

The major, trace and rare earth element patterns of the granitoids also support the isotopic results. K contents of the granites increase from the old series to the young series. This is particularly evident for LREE, Rb, Ba, Pb, and Th. They collectively support crustal contribution in the SMG.

The Eocene and Miocene plutons have major and trace element characteristics that are comparable in many respects to typical volcanic arc and/or collision granites. However, the tectonic evolution of the region, as discussed in the light of the regional geological data, indicates that the subduction of the northern branch of the Neo-Tethys Ocean had long been completed before the Eocene by the collision of the Sakarya zone along the İzmir-Ankara-Erzincan suture (Yılmaz et al. 1995). Therefore the magmas must have been originated, not above an active subduction zone but from lithospheric mantle lying beneath the North Western Anatolian crust that was enriched during the earlier subduction event. The differences between the Eocene and the Miocene series do not imply major changes in the geodynamic environment. The trend from low-K, calc-alkaline, and low Sr isotopic ratios to high-K, calc-alkaline, and high Sr isotopic ratios from the Eocene to the Miocene is compatible with a progressive increase in the contribution of crust over time. Another explanation may be that difference in the degree of metasomatism of the source may have caused a similar picture. To differentiate between the two explanations requires a further study.

The high Ba–Sr granitoids closely resemble other continental collisional zones where removal by delamination of the lower part of thickened lithospheric mantle is regarded widely as the cause of post-collisional magmatism. The raising geotherms may have triggered partial melting to form potassium-rich magmas, some of which later differentiated into the high Ba–Sr granitoids (Tarney and Jones 1994; Fowler et al. 2001).

Perturbation of subduction-metasomatized lithosphere either by delamination of the thermal boundary layer or by slab detachment may have generated the hot, primary magmas, which were emplaced into thick continental crust as small magma batches. A similar mechanism was also proposed for the generation of the collision-related magmatics for eastern, western, and central Anatolian regions (Pearce et al. 1990; Keskin et al. 1998; Aldanmaz et al. 2000; Keskin 2003; İlbeyli et al. 2004).

Recently, "slab breakoff" model was used to to explain why syn-collisional magmatism preceded the subduction in many collisional magmatic belts, such as late Caledonian magmatism in Ireland (Atherton and Ghani 2002) and Neogene magmatism of the Mediterranean Maghreb margin (Maury et al. 2000). The western part of the Alpine–Himalayan orogenic belt; Alpine Tertiary magmatism (Davies and von Blanckenburg 1995) and in the eastern edge of the belt; the Greater Himalayan sequence magmatism (Kohn and Parkinson 2002) are also explained by the slab breakoff model.

Generation of a linear belt of Eocene granitoids with hybrid geochemical features and high-K Miocene magmatism may also be explained by the slab breakoff model, because this region is also located along the Alpine–Himalayan orogenic belt. According to this model the linear heat pulse above the broken slab produced small volume melts that emplaced as separated plutons in south Marmara region.

Conclusions

The South Marmara region contains two granitoid belts: an older belt of Eocene age (OGB) and a younger belt of Miocene age (YGB). The OGB is located in the north, trends E–W trending belts, is the more primitive, and is mainly represented by intrusive bodies. The YGB is represented by volcano–plutonic complexes and is located in the south.

The main characteristic features of the two series may be summarized as follows. The OGB were formed from several magma pulses covering a wide compositional spectrum from medium-K diorites to granites and formed within a wide time interval (36–45 Ma). The YGB consists of high-K quartz monzonite, granodiorite, and associated lavas which have a narrow compositional range and formed within a narrower time interval (19–23 Ma).

The OGB were emplaced into basement rocks and produced contact metamorphism reaching the hornblende-pyroxene hornfels facies. These data together with the lack of associated volcanic rocks suggest that they were emplaced in deeper levels in the crust possibly at a depth below 5 km. The contact migmatites formed around the northern rim of the OGB Kapıdağ pluton further support this assumption.

The OGB, on the other hand, which display close interaction and transition to high-grade metamorphic rocks as they collectively form composite magmatic bodies indicate that they were emplaced at much deeper levels in the crust compared to the YGB. The overlying rocks of OGB must have been removed either by erosional or tectonic removal or by both, which allowed the granites to croup out stripping of the cover rocks must have occurred between the Early Miocene and the Late Miocene period, because the granite is stratigraphically overlain by the extensive outcrops of lacustrine limestone of the late Miocene age. The absence of the overlying rocks in the region of OGB suggests that this region was elevated at a rate higher than the region where YGB crop out, and possibly tilted towards the south. Consequently the northern part of the region has undergone much severe tectonic and/or erosional removal of the cover units.

The geochemistry of the SMG and the geodynamic features of the region indicate that the SMG originated as a result of the continental collision and that the mantle lith-

osphere underlying this region was geochemically modified by earlier subduction. During the ascent and storage the mantle-derived magmas experienced crustal assimilation and contamination. AFC models show that crustal contribution increases from north to south.

Acknowledgments We acknowledge the Scientific and Technical Research Council of Turkey (TUBITAK: project code YDABÇAG-101Y007) for supporting the field study and geochemical analyses. Z. Karacık also thanks Ö.F. Gürer for help during the fieldwork. Dr. Judith Bunbury and anonymous reviewer provided very constructive comments on the manuscript.

Appendix: Analytical techniques

Major and trace elements were determined at Cardiff University. Samples were ignited at 900°C in a muffle furnace to determine loss on ignition. 0.1 g of ignited powder were fused with 0.4 g of Li-metaborate, and the resulting melts were dissolved and taken up in 100 ml of 2% HNO_3. Sample solutions were analyzed by inductively coupled plasma-optical emission spectrometry (ICP-OES) using a JY Horiba Ultima 2 ICP-OES system. Calibration was performed using international reference materials BIR-1, W2, MRG-1, JA2, and JG3. Instrumental precision varied between 0.2 and 8.5% depending on the elemental concentration present. Accuracy was determined by repeat analysis of separate (user-prepared) solutions of W2 and JA2 and of the international granite standard GSP-1. Results were consistently within 5% of the accepted values.

For isotope analyses, Rb, Sr, and light rare-earth elements were isolated on quartz columns by conventional ion exchange chromatography with a 5 ml resin bed of Bio Rad AG 50W-X12, 200–400 mesh. Nd was separated from other rare-earth elements on quartz columns using 1.7 ml Teflon powder coated with HDEHP, di(2-ethylhexyl) orthophosphoric acid, as cation exchange medium. All isotopic measurements were made by Thermal Ionization Mass Spectrometry, on a Finnigan MAT 262 mass spectrometer at Tübingen University. Sr was loaded with a Ta-HF activator on pre-conditioned W filaments and was measured in single-filament mode. Nd was loaded as phosphate on pre-conditioned Re filaments, and measurements were performed in a Re double filament configuration. The $^{87}Sr/^{86}Sr$ isotope ratios were normalized to $^{86}Sr/^{88}Sr = 0.1194$ and the $^{143}Nd/^{144}Nd$ isotope ratios to $^{146}Nd/^{144}Nd = 0.7219$. Analyses of 21 separate loads of Ames metal, (Geological Survey of Canada; Roddick et al. 1992), during the course of this study (01-07/2003) gave a $^{143}Nd/^{144}Nd$ of 0.512141 ± 0.000020 (± errors are 2-sigma of the mean) and within the same period the NBS 987 Sr standard yielded a $^{87}Sr/^{86}Sr$ of 0.710248 ± 0.000021 ($n = 29$). Total procedural blanks (chemistry and loading) were <200 pg for Sr and <50 pg for Nd.

The K/Ar age determinations has been done at Activation (geochronology and isotopic geochemistry) laboratories. The K concentration was performed by ICP. The argon analysis was performed using the isotope dilution procedure on noble gas mass spectrometry. An aliquot of the sample is weighted into Al container, loaded into sample system of extraction unit, degassed at ~100°C during 2 days to remove the surface gases. Argon is extracted from the sample in double vacuum furnace at 1,700°C. Argon concentration is determined using isotope dilution with ^{38}Ar spike, which is introduced to the sample system prior to each extraction. The extracted gas is cleaned up in two-step purification system. Then pure Ar is introduced into customer build magnetic sector mass spectrometer (Reinolds type) with Varian CH5 magnet. The ion source has an axial design (Baur-Signer source), which provides more than 90% transmission and extremely small isotopic mass-discrimination. Measurement Ar isotope ratios is corrected for mass-discrimination and then atmospheric argon is removed assuming that ^{36}Ar is only from the air. Concentration of ^{40}Ar radiogenic is calculated by using ^{38}Ar spike concentration. After each analysis the extraction temperature is elevated to 1,800°C for few minutes and furnace is prepared for next analysis. K-analysis; aliquot of the sample is weighted into graphite crucible with lithium metaborate/tetraborate flux and fussed using LECO induction furnace. The fusion bead is dissolved with acid. Standards, blanks, and sample are analyzed on Thermo Jarrell Ash Enviro II ICP Spectrometer.

References

Aksoy R (1995) Stratigraphy of the Marmara Island and Kapıdağ Peninsula. Turk Assoc Pet Geol Bull 7–1:33–49

Aldanmaz E, Pearce JA, Thirlwall MF, Mitchell JG (2000) Petrogenetic evolution of late Cenozoic, post-collision volcanism in western Anatolia, Turkey. J Volcanol Geotherm Res 102:67–95

Altunkaynak Ş, Yılmaz Y (1998) The Mount Kozak magmatic complex, Western Anatolia. J Volcano Geotherm Res 85(1–4):211–231

Ataman G. (1974) Revue geochronoloqique, des massifs plutoniques et metamorphiques de l'Anatolie. Hacettepe Bulletin of Natural Sciences and Engineering 3:518–523

Atherton MP, Ghani AA (2002) Slab breakoff: a model for Caledonian, Late Granite syn-collisional magmatism in the orthotectonic (metamorphic) zone of Scotland and Donegal, Ireland. Lithos 62:65–85

Bingöl E (1976) Biga yarımadasının jeolojisi ve Karakaya formasyonunun bazı özellikleri. Cumhuriyetin 50. yılı Yerbilimleri kongresi, Tebliğler kitabı, MTA, 70–75

Bingöl E, Delaloye M, Ataman G (1982) Granitic intrusion in Western Anatolia: a contribution to the geodynamic study of this area. Eclogae Geol Helv 75(2):437–446

Cox KG, Bell JD, Pankhurst RJ (1979) The interpretation of igneous rocks. George Allen& Unwin, Boston

Davies JH, von Blanckenburg F (1995) Slab breakoff, a model of lithosphere detachment and its test in the magmatism and deformation of collisional orogens. Earth Planet Sci Lett 129:85–102

Delaloye M, Bingöl E (2000) Granitoids from western and northwestern Anatolia: geochemistry and modeling of geodynamic evolution. Int Geol Rew 42:241–268

De Paolo DJ (1981) Trece element and isotopic effects of combined wall rock assimilation and fractional crystallization. Earth Planet Sci Lett 53:189–202

Emre O, Erkal T, Kazancı N, Görmüş S, Görür N (1997) Güney Marmara'nın Neojen ve Kuvaterner'deki Morfotektoniği. In: Güney Marmara Bölgesinin Neojen ve Kuaterner Evrimi, TUBİTAK YDABC, AG-426/G Proje Raporu, pp 36–68 (Open File Rep)

Fowler MB, Henney PJ, Darbyshire DPF, Greenwood PB (2001) Petrogenesis of high Ba–Sr granites: the Rogart plutons, Sutherland. J Geol Soc Lond 158:521–534

Genç ŞC (1998) Evolution of the Bayramiç magmatic complex, northwestern Anatolia. J Volcano Geotherm Res 85(1–4):233–249

Genç ŞC, Yılmaz Y (1995) Evolution of the Triassic continental margin, Northwest Aatolia. Tectonophysics 243:193–207

Genç ŞC, Yılmaz Y (1997) An example of post-collisional magmatism in Northwestern Anatolia: the Kızderbent volcanic (Armutlu peninsula, Turkey). Tr J Earth Sci 6:33–42

Güleç N (1991) Crust–mantle interaction in western Turkey: implications from Sr and Nd isotope geochemistry of Tertiary and Quaternary volcanics. Geol Mag 128(5):417–435

Gülen L (1990) Isotopic characterisation of Aegean magmaism and geodynamics evolution of the Aegean subduction. In: Proc Int Earth Sci Congr Aegean regions, İzmir, pp 143–166

Goldstein SL, O'Nions RK, Hamilton PJ (1984) A Sm–Nd isotopic study of atmospheric dusts and particulates from major river systems. Earth Planet Sci Lett 70:221–36

Grove TL, Donnelly Nolan JM, Housh T (1997) Magmatic processes that generated the rhyolite of Glass Mountain, Medicine Lake Volcano, N California. Contrib Mineral Petrol 127(3):205–223

Harris NBW, Pearce JA, Tindle AG (1986) Collision tectonics. Geological Society Special Publication No. 19

Harris N, Kelley S, Okay AI (1994) Post-collisional magmatism and tectonics in northwest Anatolia. Contrib Mineral Petrol 117:241–252

Hawkesworth CJ (1982) Isotope characteristics of magmas erupted along destructive plate margins. In: Thorpe RS (ed) Orogenic Andesites and related rocks. Wiley, New York, pp 549–571

Hildreth W, Moorbath S (1988) Crustal contribution to arc magmatism in the Andes of southern Chile. Contrib Mineral Petrol 98:455–489

İlbeyli N, Pearce JA, Thirlwall MF, Mitchell JG (2004) Petrogenesis of collision-related plutonics in Central Anatolia, Turkey. Lithos 72:163–182

Karacık Z, Yılmaz Y (1998) Geology of the ignimbrites and the associated volcano-plutonic complex of the Ezine area, northwestern Anatolia. J Volcan Geotherm Res 85(1–4):251–264

Keskin M (2003) Magma generation by slab steepening and breakoff beneath a subduction-accretion complex: an alternative model for colision-related volcanism in Eastern Anatolia, Turkey. Geophys Res Lett 30(24):8046

Keskin M, Pearce JA, Mitchell JG (1998) Volcano-stratigraphy and geochemistry of collisin-related volcanism on the Erzurum-Kars Plateau, northeastern Turkey. J Volcanol Geotherm Res 85:355–404

Kohn MJ, Parkinson CD (2002) Petrologic case for Eocene slab breakoff during the Indo-Asian collision. Geology 30:591–594

Köpübaşı N, Aldanmaz E (2004) Geochemical constrains on the petrogenesis of Cenozoic I-type granitoids in Northwest Anatolia, Turkey: evidence for magma generation by lithospheric delimination in a post-collisional setting. Int Geol Rev 46:705–729

Langmuir CH, Vocke RD, Hanson GN Jr (1978) A general mixing equation with applications to Icelandic basalts. Earth Planet Sci Lett 37:380–392

Maniar PD, Piccoli PM (1989) Tectonic discrimination of granitoids. Geol Soc Am Bull 101:635–643

Maury RC, Fourcade S, Coulon C, Al Azzouzi M, Bellon H, Coutelle A, Ouabadi A, Semroud B, Megartsi M, Cotten J, Belanteur O, Louni-Hacini A, Pique A, Capdevila R, Hernandez J, Rehault JP (2000) Post-collisional Neogene magmatism of the Mediterranean Maghreb margin: a consequence of slab breakoff. Earth Planet Sci 331:159–173

Miyashiro A (1978) Nature of alkalic volcanic rock series. Contrib Mineral Petrol 66:91–104

Okay AI, Satır M (2000) Coeval plutonism and metamorphism in a latest Oligocene metamorphic core complex in northwest Turkey. Geol Mag 137(5):495–516

Okay AI, Siyako M, Bürkan KA (1990) Biga yarımadasının jeolojisi ve tektonik evrimi. TPJD Bülteni C.2/1:83–121

Okay AI, Satır M, Maluski H, Siyako M, Metzger R, Akyüz S (1996) Paleo-and Neo-Tethyan events in Northwest Turkey: geological and geochronological constrains. In: Yin A, Harrison TM (eds) The tectonic evolution of Asia. Cambridge University Press, Cambridge, pp 420–441

Okay AI, Tansel I, Tüysüz O (2001) Obduction, subduction and colision as reflected in the Upper Cretaceous–Lower Eocene sedimantary record of western Turkey. Geol Mag 138:117–42

Pearce JA (1983) Role of the sub-continental lithosphere in magma genesis at active continental margins. In: Hawkesworth CJ, Norry MJ (eds) Continental basalts and Mantle Xenoliths, Shiva Publication, Cheshire, pp 230–249

Pearce JA, Harris NBW, Tindle AG (1984) Trace element discrimination diagrams for the tectonic interpretation of granitic rocks. J Petrol 25(4):956–938

Pearce JA, Bender JF, DeLong SE, Kidd WSF, Low PJ, Güner Y, Şaroğlu F, Yılmaz Y, Moorbath S, Mitchell JG (1990) Genesis of collision volcanism in eastern Anatolia, Turkey. J Volcanol Geotherm Res 44:189–229

Roddick JC, Sullivan RW, Dudás FÖ (1992) Precise calibration of Nd tracer isotopic composition for Sm–Nd studies. Chem Geol 97:1–8

Şaroğlu F, Emre O, Kuşçu I (1992) Türkiye Diri Fay Haritası (Active fault map of Turkey), scale 1:2,000,000 one sheet. Maden Tekik Arama Genel Müdürlüğü, Ankara

Şengör AMC, Yılmaz Y (1981) Tethyan evolution of Turkey: a plate tectonic approach. Tectonophysics 75:181–241

Şengör AMC, Yılmaz Y, Sungurlu O (1984) Tectonics of the Mediterranean Cimmerides: nature and evolution of the western termination of Paleo-Tethys. Geol Soc Lond Spec Publ 17:77–112

Sun SS, McDonough WF (1989) Chemical and isotopic systematic of oceanic basalts: implications for mantle composition and processes, In: Saunders AD, Norry MJ (eds) Magmatism in the ocean basins. Geological Society of London Special Publication no. 42, pp 313–345

Tarney J, Jones CE (1994) Trace-element geochemistry of orogenic igneous rocks and crustal growth-models. J Geol Soc 151(part 5):855–868

Taylor HP (1980) The effects of assimilaton of country rocks by magmas on $^{18}O/^{16}O$ and $^{87}Sr/^{86}Sr$ systematics in igneous rocks. Earth Planet Sci Lett 47:243–254

Thirlwall MF, Jones NW (1983) Isotope geochemistry and contamination mechanics of Tertiary lavas from Skye, Northwest Scotland. In: Hawkesworth CJ, Norry MJ (eds) Continental Basalts and Mantle Xenoliths. Shiva Publishing, Cheshire, pp 186–208

Voshage H, Hofmann AW, Mazzucchelli M, Rivalenti G, Sinigoi S, Raczek I, Demarchi G (1990) Isotopic evidence from the Ivrea zone for a hybrid lower crust formed by magmatic underplating. Nature 347:731–736

Yılmaz Y (1989) An approach to the origin of young volcanic rocks of western Turkey. In: Şengör AMC (ed) Tectonic evolution of the Tethyan Region. Kluwer, Dordrecht, pp 159

Yılmaz Y (1990) Comparisons of the young volcanic associations of the west and the east Anatolia under the compressional regime: a review. J Volcanol Geotherm Res 44:69–87

Yılmaz Y (1997) Geology of western Anatolia. Active tectonics of northwestern Anatolia. The Marmara poly-project, a multidisciplinary approach by space-geodesy, geology, hydrogeology, geothermic and seismology. Vdf Hochschulverlag AG an der Zurich, pp 31–53

Yılmaz Y, Genç ŞC, Yiğitbaş E, Bozcu M, Yılmaz K (1995) Geological evolution of the late Mesozioc continenetal margin of northwestern Anatolia. Tectonophysics 243:155–171

Yılmaz Y, Genç ŞC, Gürer F, Bozcu M, Yılmaz K, Karacık Z, Altunkaynak Ş, Elmas A (2000) When did the western Anatolian grabens begin to develop? In: Bozkurt E, Winchester JA, Piper JDA (eds) Tectonic and magmatism in Turkey and surrounding area. Geol Soc Special Publication 173:353–384

Yılmaz Y, Genç ŞC, Karacık Z, Altunkaynak Ş (2001) Two contrasting magmatic associations of NW Anatolia and their tectonic significance. J Geodyn 31:243–271